Journal of Power Sources 434 (2019) 226727

Contents lists available at ScienceDirect

Journal of Power Sources

journal homepage: www.elsevier.com/locate/jpowsour

In-operando imaging of polysulfide catholytes for Li–S batteries and implications for kinetics and mechanical stability

Yuwei Zhang, Coleman Fincher, Scott McProuty, Matt Pharr *

Department of Mechanical Engineering, Texas A&M University, College Station, TX, 77840, USA

HIGHLIGHTS

- We optically observe morphological changes during cycling of polysulfide catholyte.
- Varying the charging rate induces varying morphology during cycling.
- The stress developed during lithiation decreased with increasing charge rate.
- We connect the stress changes to morphological changes as a function of charge rate.

GRAPHICAL ABSTRACT

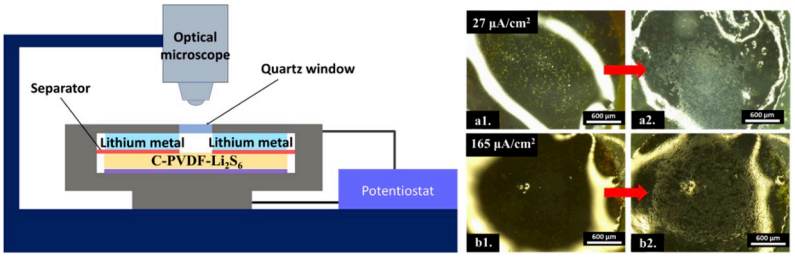

ARTICLE INFO

Keywords:
In-operando
Lithium polysulfide catholyte
In-situ stress measurement
Lithium sulfur battery

ABSTRACT

Enhancing the electrochemical performance of lithium-sulfur batteries requires improved fundamental understanding of the reduction and oxidation of the soluble lithium polysulfide species. To this end, we have designed a 'donut-shaped' cell to enable direct optical observation of phase transformations of a liquid polysulfide catholyte to solid lithium sulfide during electrochemical cycling. We use this technique to image the spatio-temporal distribution of the solid lithium sulfide as it deposits on a carbon matrix at different charging rates. These experiments indicate that the reduction and oxidation of polysulfide catholyte occurs as a thin film deposition and growth process during both lithiation and delithiation. We then investigate the ramifications of these morpological changes in terms of mechanical stability by measuring the evolution of stress during discharge of the polysulfide catholyte. The stress measurements indicate that the average stress during discharging decreases with increasing the charging rate, which we attribute to less dense deposition of lithium sulfide at high discharge rates.

1. Introduction

With the world's population increasing and technology advancing, demands continue to increase for energy dense storage materials. Lithium sulfur batteries have attracted much attention due to their enormous theoretical capacity (1672 mAh/g) and energy density (~2500 Wh/kg), which is an order of magnitude larger than existing transition-metal cathodes (e.g., $LiCoO_2$, $LiFePO_4$, $Li(Ni_xMn_yCo_{1-x-y})O_2$) [1–5]. Combined with its abundance in the earth's crust, sulfur represents a promising low cost, light weight, and relatively environmentally benign candidate material for cathodes of Li-based batteries [6–8].

Despite these promising attributes, a host of issues exist that result in degradation of sulfur batteries, from the loss of active material due to shuttling of electrolyte-soluble polysulfides to the insulating nature of

* Corresponding author.
E-mail address: m-pharr@tamu.edu (M. Pharr).

https://doi.org/10.1016/j.jpowsour.2019.226727
Received 9 March 2019; Received in revised form 9 May 2019; Accepted 3 June 2019
0378-7753/© 2019 Elsevier B.V. All rights reserved.

both sulfur and Li_2S (both electronically and ionically) resulting in poor utilization of active material [9,10]. Additionally, as a high-capacity electrode, sulfur suffers severe structural distortions (solid-to-liquid, liquid-to-liquid, and solid-to-liquid phase transformations) intrinsic to the discharge/charge process [10,11]. Correspondingly, the complicated conversion reactions produce an enormous volume expansion (~80%), which can lead to a loss of contact between the insulating active materials and the conductive carbon matrix [12]. These inactive layers eventually spread, producing a barrier for further lithium ion transport, and ultimately leading to capacity fade [13].

To address these issues, recent studies have implemented soluble lithium polysulfides encapsulated by porous carbon frameworks as an alternative to using solid sulfur as the active material. These systems have demonstrated more uniform distribution of active material and more intimate contact to the carbon-based matrices [14–16]. This configuration will also likely leads to enhanced kinetics since it avoids the initial solid to liquid phase transformation from S_8 to Li_2S_8 [17]. Overall utilizing a modified conductive carbon matrix as the host material and dissolved lithium polysulfides as the active material, several groups have demonstrated high-performance batteries with low polarization, high areal capacity, and promising cycling performance [18–21].

Despite these advances, a full understanding of the conversion from soluble polysulfides to solid lithium sulfide is lacking. In particular, direct observation of when/where solid species form during discharge would provide insight into the conversion process. Likewise, the details of the morphological evolution are intimately connected to stresses that develop during cycling. Understanding these links would provide guidance into the design of host materials and cycling conditions that mitigate mechanical damage, thereby promoting stable cycling. To fill these gaps in knowledge, we construct a simple in-operando lithium-sulfur 'donut cell' design, which enables the user to directly image the spatio-temporal distribution of solid lithium sulfide species during electrochemical cycling. We also perform in-situ measurements of mechanical stresses generated during electrochemical discharge of a polysulfide catholyte, i.e., during deposition of lithium sulfide onto a host carbon matrix. These experiments provide key insight into the lithiation/delithiation process of polysulfide catholytes and establish a technique for future characterization of various catholytes under various electrochemical cycling conditions.

2. Materials and methods

2.1. Electrochemical cell preparation

A spin coating process prepared conductive matrices, using carbon nanoparticles (99.99% US Research Nanomaterials, Inc.) as the conductive component, and polyvinylidene fluoride (PVDF, MTI Corporation) as the binder in a 6:1 (C: PVDF) mass ratio. Mixing these components into solution using N-Methyl-2-pyrrolidone (NMP, MTI Corporation) as a solvent, followed by magnetic stirring for 3 h produced a slurry. Spin coating at 1000 rpm for 1 min deposited the slurry onto mirror-finished T304 stainless steel (Metals Depot). After spin coating, the resulting film dried at 45 °C for 3 h. A profilometer (Veeco Dektak 150 Profilometer) provided measurements of the thickness of the composite carbon matrix. We should note that by integrating C-nanoparticles in a manner that produces overall porosity, we are implementing shapes (interconnected porous structure) and sizes (nanometer scale features) that are representative of typical geometries used in Li–S systems [15,22–26].

To prepare the polysulfide catholyte, sulfur nanoparticles (99.99% US Research Nanomaterials Inc) and lithium sulfide (Li_2S, 99.98% trace metals basis) were mixed in an appropriate molar ratio in a solution of 1,3-dioxolane (DOL, Sigma-Aldrich) and 1,2-dimethoxyethane (DME, Sigma-Aldrich) (volume ratio = 1:1) with the addition of 0.5 wt% $LiNO_3$ (Sigma-Aldrich) as an additive, thereby rendering a 1 M Li_2S_6 solution (molar concentration calculated based on the mass of sulfur). Heating this mixture at 55 °C overnight produced a dark brown solution. For the blank electrolyte (i.e., the one with no dissolved polysulfide), dissolving 1.0 M lithium bis-trifluoromethanesulphonylimide (LiTFSI, Sigma-Aldrich) in a 1:1 by volume solution of 1,3-dioxolane (DOL, Sigma-Aldrich): 1,2-dimethoxyethane (DME, Sigma-Aldrich), with the addition of 0.5 wt% $LiNO_3$ as an additive (Sigma-Aldrich) produced the blank electrolyte. We used a precision electronic single channel pipette (MTI Inc.) to withdraw 20 μL of catholyte for each test. As such, the equivalent mass we used for each test is 0.64 mg.

A two-electrode electrochemical test cell with a quartz viewing window (MTI Corporation) facilitated simultaneous electrochemical and mechanical measurements, as depicted in Fig. 1. We assembled this cell in an argon-filled glovebox with oxygen and moisture levels less than 0.1 ppm. Adding polysulfide catholyte (1 M Li_2S_6) into the composite carbon matrix produced the C-PVDF-Li_2S_6 composite electrode. We then put a Celgard 2400 separator (MTI Corporation) on top of the cathode following by adding blank electrolyte. Finally, placing a lithium metal ribbon (99.9% trace metals basis, Sigma-Aldrich) on top of the separator produced the anode.

2.2. Electrochemical measurements

A PARSTAT MC Multichannel Potentiostat (Princeton Applied Research) conducted galvanostatic cycling at various current densities between the open circuit potential to 1.8 V vs Li/Li+. All experiments occurred at room temperature (25 °C).

2.3. Mechanical characterization

A multibeam optical stress sensor (MOS) from k-Space Associates monitored the curvature of the substrate (ΔK) during electrochemical cycling, as shown in Fig. 1. The MOS employs an array of parallel laser beams to measure the curvature of the substrate of the composite cathode. The array of laser beams allows simultaneous illumination and detection, which in turn greatly reduces noise in the measurements caused by fluid motion in the electrochemical cell or by ambient vibrations. The cell is also placed on an antivibration table during testing. Using Stoney's equation, we deduced the average stress change in the composite cathode during cycling [27,28],

$$\Delta\sigma = \frac{E_s h_s^2}{6h_f(1-\nu_s)}\Delta K,$$

where E_s is the elastic modulus of the substrate (E_s = 203 GPa), h_s is the thickness of the substrate (h_s = 0.736 mm), ν_s is the Poisson's ratio of the substrate (ν_s = 0.29), and h_f is the thickness of electrode film (measured via profilometry before the test). In this study, we take h_f as constant for each test, such that the stress calculated is the nominal in-plane stress. A previous study has shown that the thickness of a similar porous composite sulfur thin film cathode fabricated through a slurry method remains constant during electrochemical cycling [29].

2.4. In-operando optical imaging

Assembly of the batteries for these studies occurred as in Section 2.1 except that cutting the separator and lithium foil into a 'donut' shape opened an optical viewing path to the surface of the cathode (see Fig. 2). A VHX-600 Digital Microscope captured images every 15 s to monitor the evolution of the surface morphology during electrochemical cycling at various charging rates.

3. Results and discussion

Fig. 3 shows the change in potential during galvanostatic cycling of a lithium polysulfide catholyte (Li_2S_6) at 165 μA/cm^2. During both discharge and charge, a number of phase transformations occur (as

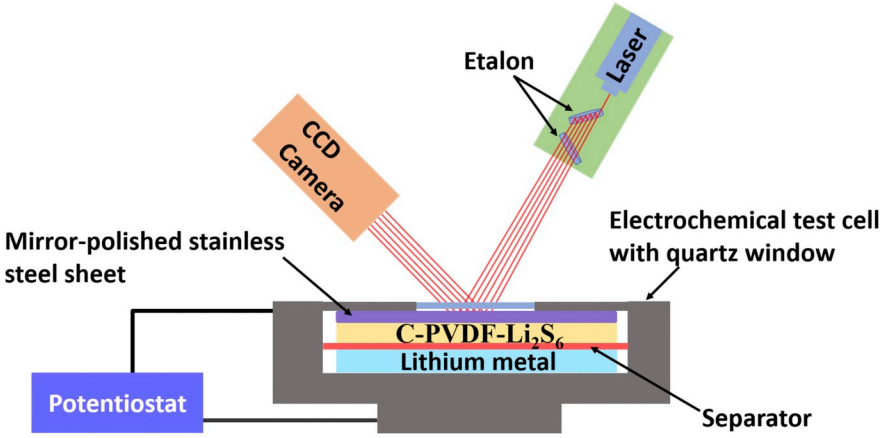

Fig. 1. A schematic representation of the electrochemical test, which employs a split cell with a quartz viewing window through which the use of an in-situ multibeam optical sensor enables measurements of stress during electrochemical cycling.

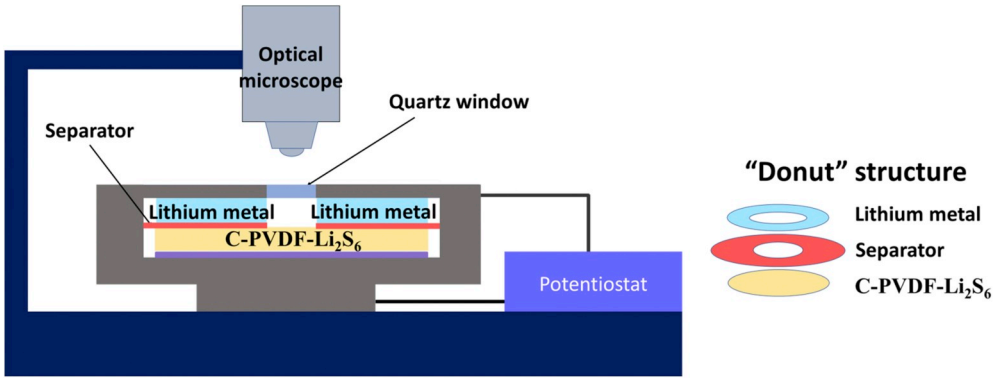

Fig. 2. A schematic representation of the electrochemical setup in which in-operando optical microscopy enables imaging of morphological changes during electrochemical cycling. Cutting the Li metal and separator in to a 'donut' shape opened an optical viewing path to the surface of the cathode.

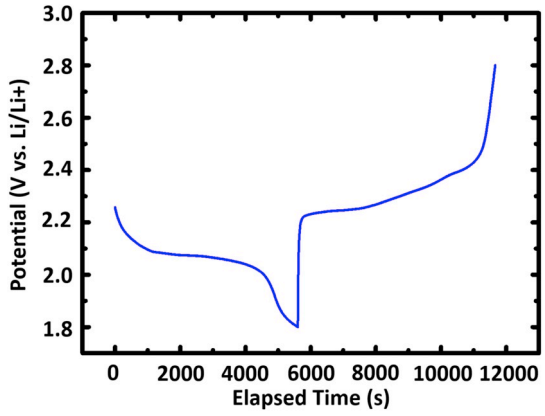

Fig. 3. Representative potential response of Li_2S_6 polysulfide catholyte during galvanostatic lithiation/de-lithiation at a current density of 165 μA/cm^2.

indicated by voltage plateaus), which are substantially more complex than standard intercalation cathodes, such as $LiFePO_4$, $LiCoO_2$, and Li$(Ni_xMn_yCo_{1-x-y})O_2$ [4,5,30]. To better understand this complicated cycling process, we monitored the changes in morphology of the surface of the C-PVDF-Li_2S_6 cathode during lithiation/de-lithiation at two different charging rates. Additionally, to connect this morphological evolution to potential mechanical issues, we measured the evolution of mechanical stresses during discharge at various current densities to paint a full picture of how kinetics, morphology, and mechanics interact during operation of polysulfide catholytes.

3.1. *Morphological evolution during lithiation at different current densities*

Fig. 2 shows the experimental setup used to monitor the morphological evolution during electrochemical cycling of a carbon matrix soaked with polysulfide catholyte (C-PVDF-Li_2S_6). Using this setup, Fig. 4 shows optical images of the morphology of the polysulfide catholyte before and after the first lithiation at current densities of 27 μA/cm^2 (a1-a2) and 165 μA/cm^2 (b1-b2) (for the full-time evolution, see the Videos S1 and S2 in the supporting information). The curved bright lines around the periphery of these images occur from light reflecting off of the separator in the battery. In these two sets of images (and the corresponding videos), we observe that the solid phase deposited as islands, which gradually grew and coalesced into a relatively large region that covers the majority of the center region. Within the deposited regions, the lithium sulfide generally packed less densely at higher current densities, i.e., less densely in Fig. 4-b2 as compared to Fig. 4-a2. Several papers have discussed the phase transformation corresponding to the 2.1 V voltage plateau, which represents a liquid-to-solid phase transformation with relatively slow kinetics [31–33]. In this study, Fig. 4 and Videos S1 and S2 (supporting information) show direct evidence that lithiation of the polysulfide catholyte at a voltage plateau near 2.1 V occurs via a thin film nucleation and growth process of the solid phase. Moreover, using a larger current density results in the system having insufficient time for the growth process to fully occur, thereby producing a relatively low density of lithium sulfide and correspondingly low

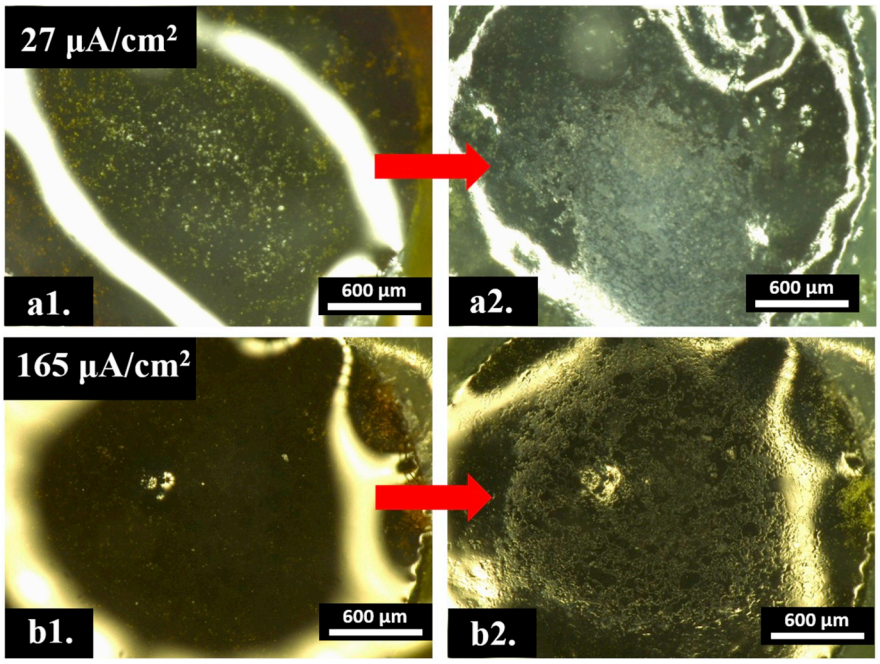

Fig. 4. Optical microscopy images of C-based matrices soaked with polysulfide catholyte during the first lithiation. (a1) Before (a2) after lithiation at a current density of 27 μA/cm^2. (b1) Before and (b2) after lithiation at a current density of 165 μA/cm^2

capacities. As such, our studies underscore the importance of understanding the precise mechanisms of this growth process. Doing so would provide insight into defining host matrix chemistries and geometries, charging conditions, and catholyte chemistries (e.g., additives) that would enhance the kinetics of the growth process, and thereby should represent a key area of research going forward.

Supplementary video related to this article can be found at https://doi.org/10.1016/j.jpowsour.2019.226727.

As a final note, although we believe our experimental setup accurately mimics a realistic environment of oxidation and reduction of polysulfides, the reaction process in a more standard electrochemical cell (without 'donut' holes in the center of separator and lithium metal ribbon) may vary somewhat since the kinetics for polysulfide deposition and dissolution may differ between the region near the edge of the 'donut' and in the center of the 'donut'. However, based on general similarity observed herein to morphologies seen in previous studies, we believe our technique provides useful information regarding the general changes in morphology under various conditions [29,34]. For instance, in a previous study [29], we surmised that the 2.1 V voltage plateau corresponds to a nucleation and growth type phase transformation.

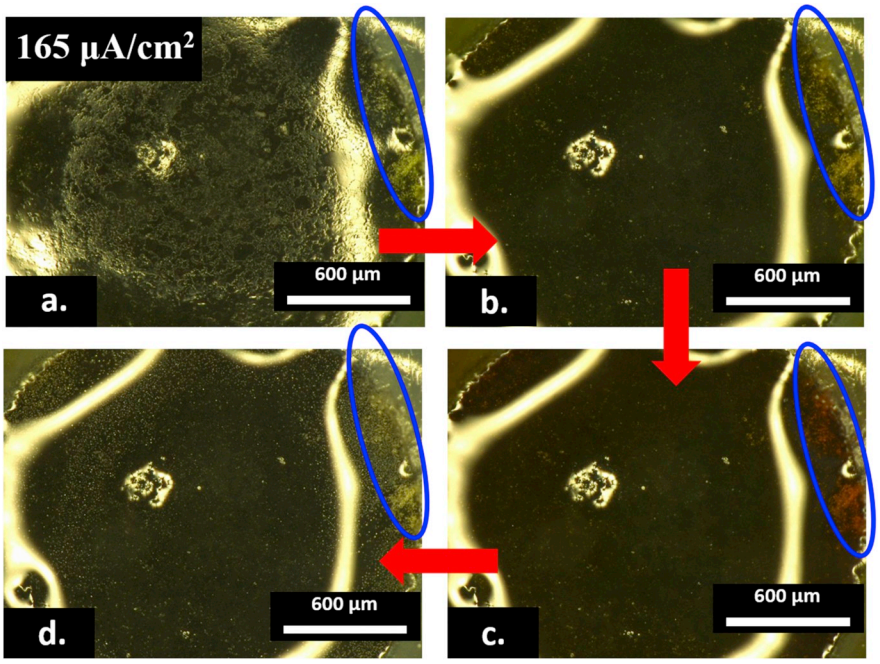

Fig. 5. Optical microscopy images of C-based matrices soaked with polysulfide catholyte at different states during delithiation at a current density of 165 μA/cm^2. (a) Represents the start and (d) represents the end of delithiation. (b) and (c) are intermediate points chosen based on interesting morphological features. The blue circles highlight an area of interest. (For interpretation of the references to color in this figure legend, the reader is referred to the Web version of this article.)

Videos S1–S3 (supporting information) provide direct evidence of the time evolution of this nucleation and growth process. Also, compared to in-situ TEM studies, our technique is relatively simple in terms of sample preparation and provides a much larger field of view [35,36].

Supplementary video related to this article can be found at https://doi.org/10.1016/j.jpowsour.2019.226727.

3.2. Morphological evolution during de-lithiation

Fig. 5 shows the morphological evolution of a polysulfide catholyte during delithiation at a current density of 165 μA/cm^2. These images correspond to the same electrode as shown in Fig. 4 b1-b2. The full time-lapsed Video S3 of this reaction is also included in the supporting information. In a previous study [29], we surmised that near the end of de-lithiation, a solid phase of sulfur will deposit back onto the carbon matrix in a thin film nucleation and growth type process. Fig. 5 and Video S3 (supporting information) provide direct observation of the time evolution of this nucleation and growth process. Specifically, at the beginning of delithiation, solid lithium sulfide exists on the carbon matrix (Fig. 5a). Upon delithiation, the solid phases disappeared completely, indicating their dissolution into the electrolyte (see Fig. 5b). With further delithiation, different dissolved polysulfides form (Li_2S_4, Li_2S_6, Li_2S_8) in the center region, such that Fig. 5c appears similar to that of Fig. 5b. However, in the circled region near the top right corner in Fig. 5c, some reddish liquid appears, different from that of the previous images. As reported in several previous studies, with further delithiation, the color of polysulfide will change from light yellow to dark red upon conversion from low chain polysulfides (Li_2S_4) to high chain polysulfides (Li_2S_8), which appears to be happening here as well [37–40]. At the end of de-lithiation (Fig. 5d), the reddish liquid (Li_2S_8) disappears completely and solid particles (solid sulfur) deposit onto the carbon matrix. This final phase transformation again appears to occur through a thin film nucleation and growth process (see Video S3), as we have hypothesized in a previous study [29].

3.3. Stress evolution during lithiation at various current densities

We performed stress measurements in polysulfide-soaked carbon matrices, as to demonstrate the potential ramifications of kinetic effects in terms of mechanical stability. Fig. 1 shows the experimental setup used to measure the stress changes during electrochemical cycling. A multibeam stress sensor (MOS) monitored the change in curvature (ΔK) of the composite cathode during the process. Fig. 6 shows potential and the corresponding changes in nominal stress in the polysulfide-soaked carbon matrices during lithiation at various current densities. We conducted multiple additional tests to confirm these trends for varying current densities. Additionally, we should note that these stresses represent the average stress through the thickness of the composite cathode during lithiation. They do not provide locally differentiable information (e.g., stress in Li_2S vs. Stress in PVDF), as discussed in a previous paper [29]. However, these measurements do provide useful information regarding the overall mechanics in the system during electrochemical reactions. In a previous paper [29], we performed a systematic study related to stresses that develop during cycling of solid composite sulfur cathodes. Herein, we will focus on how the current density influences stress generated during lithiation of polysulfide catholytes.

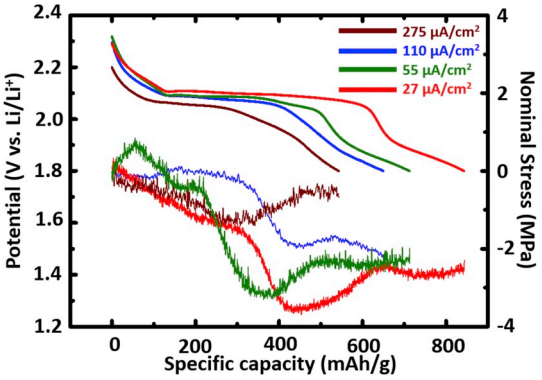

Fig. 6. Stress response during the first lithiation of C-based matrices soaked with polysulfide catholyte at different current densities.

The stress profiles demonstrate a similar general trend (i.e., shape of the curve) at various current densities. In particular, an incubation period occurs first in which the stress does not change significantly or changes with a relatively small slope. This period likely occurs due to liquid-to-liquid phase transformations or side reactions occurring during the initial stages of lithiation. This period is followed by a region in which the compressive stress increases quickly (with a relatively large slope). In this stage, nucleation and growth of the solid Li_xS phases occurs, which induces stress in the matrix. Toward the end of lithiation, the stress again appears relatively flat. This stage may occur due to additional side reactions occurring or may stem from plastic deformation occurring in the Li_xS solid phase that forms, i.e., further lithiation (i.e., straining) does not induce much additional stress. Additionally, we found that the maximum nominal stress decreased with increasing current density. This phenomenon has the opposite trend compared to that reported in Si anodes [41]. In many other systems (such as Si), the electrode remains a solid during cycling and also exhibits strain-rate sensitive constitutive behavior [4,42–44]. As such, larger charging rates produce larger strain rates and thus larger stresses [30]. By comparison, in our polysulfide catholyte battery system, when the current density increases, less of the solid phase deposits on the host matrix due to the previously discussed kinetic limitations of the growth process. With less solid phase depositing, the average stress in the system will be smaller. As a result, slower charging rates will undoubtedly increase the capacity but will also produce larger stresses, thereby again underscoring the importance of microstructural/geometric design of the host matrix to prevent mechanical damage.

4. Conclusions

In summary, this paper develops a novel technique to observe the morphological evolution in-operando during electrochemical cycling of polysulfide catholytes. We used this technique to monitor the morphological evolution of a C-PVDF matrices soaked in a polysulfide catholyte during lithiation/delithiation. These studies clearly demonstrate that solid lithium sulfide deposits onto the host C-PVDF matrices by a thin film nucleation and growth type process during lithiation. Likewise, solid sulfur deposits through a similar process during delithiation. Moreover, this growth process depends on the charging rate, with larger charging rates leading to a more inhomogeneous distribution of the deposited solid species, and thus lower capacities. We further connect these effects to potential consequences in terms of mechanical stability by performing in-operando stress measurements during lithiation of C-PVDF matrices soaked in polysulfide catholytes at various charging rates. We find that slower charging rate produces higher capacities but larger stresses, thereby underscoring the importance of microstructural/geometric design of the host matrices to prevent mechanical damage. Overall, these studies provide connections between electrochemistry and the corresponding kinetics, mechanics, and morphological phenomena associated with soluble lithium polysulfides. As such, we hope our studies will inspire future electro-chemo-mechanical models of sulfur-based batteries.

Conflicts of interest

The authors declare no competing interests.

Acknowledgements

Y. Zhang was supported by the Hagler Institute for Advanced Study (HIAS) at Texas A&M University. C. D. Fincher was supported by the National Science Foundation Graduate Research Fellowship under Grant No. 1746932. M. Pharr acknowledges funding from the mechanical engineering department at Texas A&M University and the Texas A&M Engineering Experiment Station (TEES).

References

[1] X. Ji, L.F. Nazar, Advances in Li–S batteries, J. Mater. Chem. 20 (2010) 9821.
[2] A. Manthiram, S.-H. Chung, C. Zu, Lithium-sulfur batteries: progress and prospects, Adv. Mater. 27 (2015) 1980–2006.
[3] Z.W. Seh, Y. Sun, Q. Zhang, Y. Cui, Designing high-energy lithium–sulfur batteries, Chem. Soc. Rev. 45 (2016) 5605–5634.
[4] Z. Qi, et al., LiNi0.5Mn0.3Co0.2O2/Au nanocomposite thin film cathode with enhanced electrochemical properties, Nanomater. Energy 46 (2018) 290–296.
[5] H. Liu, et al., High energy density $LiFePO_4$/C cathode material synthesized by wet ball milling combined with spray drying method, J. Electrochem. Soc. 164 (2017) A3666–A3672.
[6] G. He, X. Ji, L. Nazar, High "C" rate Li-S cathodes: sulfur imbibed bimodal porous carbons, Energy Environ. Sci. 4 (2011) 2878.
[7] X. Pu, G. Yang, C. Yu, Liquid-type cathode enabled by 3D sponge-like carbon nanotubes for high energy density and long cycling life of Li-S Batteries, Adv. Mater. 26 (2014) 7456–7461.
[8] L. Yuan, H. Yuan, X. Qiu, L. Chen, W. Zhu, Improvement of cycle property of sulfur-coated multi-walled carbon nanotubes composite cathode for lithium/sulfur batteries, J. Power Sources 189 (2009) 1141–1146.
[9] Z. Liu, A. Mistry, P.P. Mukherjee, Mesoscale physicochemical interactions in lithium–sulfur batteries: progress and perspective, J. Electrochem. Energy Convers. Storage 15 (2017), 010802.
[10] G. Zheng, Y. Yang, J.J. Cha, S.S. Hong, Y. Cui, Hollow carbon nanofiber-encapsulated sulfur cathodes for high specific capacity rechargeable lithium batteries, Nano Lett. 11 (2011) 4462–4467.
[11] Y.X. Yin, S. Xin, Y.G. Guo, L.J. Wan, Lithium-sulfur batteries: electrochemistry, materials, and prospects, Angew. Chem. Int. Ed. 52 (2013) 13186–13200.
[12] S. Waluś, et al., Volumetric expansion of Lithium-Sulfur cell during operation – fundamental insight into applicable characteristics, Energy Storage Mater 10 (2018) 233–245.
[13] S.S. Zhang, Liquid electrolyte lithium/sulfur battery: fundamental chemistry, problems, and solutions, J. Power Sources 231 (2013) 153–162.
[14] X. Pu, G. Yang, C. Yu, Trapping polysulfides catholyte in carbon nanofiber sponges for improving the performances of sulfur batteries, J. Electrochem. Soc. 162 (2015) A1396–A1400.
[15] Y. Cui, Y. Fu, Enhanced cyclability of Li/polysulfide batteries by a polymer-modified carbon paper current collector, ACS Appl. Mater. Interfaces 7 (2015) 20369–20376.
[16] L. Qie, C. Zu, A. Manthiram, A high energy lithium-sulfur battery with ultrahigh-loading lithium polysulfide cathode and its failure mechanism, Adv. Energy Mater. 6 (2016) 1–7.
[17] Y. Sun, et al., In-operando optical imaging of temporal and spatial distribution of polysulfides in lithium-sulfur batteries, Nanomater. Energy 11 (2015) 579–586.
[18] S.H. Chung, P. Han, R. Singhal, V. Kalra, A. Manthiram, Electrochemically stable rechargeable lithium-sulfur batteries with a microporous carbon nanofiber filter for polysulfide, Adv. Energy Mater. 5 (2015) 1–12.
[19] C. Zu, A. Manthiram, High-performance Li/dissolved polysulfi de batteries with an advanced cathode structure and high sulfur content, Adv. Energy Mater. 4 (2014) 2–7.
[20] C. Zu, Y. Fu, A. Manthiram, Highly reversible Li/dissolved polysulfide batteries with binder-free carbon nanofiber electrodes, J. Mater. Chem. 1 (2013) 10362–10367.
[21] G. Zhou, Y. Zhao, C. Zu, A. Manthiram, Free-standing TiO2nanowire-embedded graphene hybrid membrane for advanced Li/dissolved polysulfide batteries, Nanomater. Energy 12 (2015) 240–249.
[22] Y. Cui, Y. Fu, Polysulfide transport through separators measured by a linear voltage sweep method, J. Power Sources 286 (2015) 557–560.
[23] G. Zhou, Y. Zhao, C. Zu, A. Manthiram, Free-standing TiO2 nanowire-embedded graphene hybrid membrane for advanced Li/dissolved polysulfide batteries, Nanomater. Energy 12 (2015) 240–249.
[24] Y. Fu, Y.S. Su, A. Manthiram, Highly reversible lithium/dissolved polysulfide batteries with carbon nanotube electrodes, Angew. Chem. Int. Ed. 52 (2013) 6930–6935.
[25] G. Zhou, E. Paek, G.S. Hwang, A. Manthiram, Long-life Li/polysulphide batteries with high sulphur loading enabled by lightweight three-dimensional nitrogen/sulphur-codoped graphene sponge, Nat. Commun. 6 (2015) 1–11.
[26] C. Zu, Y. Fu, A. Manthiram, Highly reversible Li/dissolved polysulfide batteries with binder-free carbon nanofiber electrodes, J. Mater. Chem. 1 (2013) 10362–10367.
[27] G.G. Stoney, The tension of metallic films deposited by electrolysis, Proc. R. Soc. A Math. Phys. Eng. Sci. 82 (1909) 172–175.
[28] W.D. Nix, Mechanical properties of thin films, Metall. Trans. A 20 (1989) 2217–2245.
[29] Y. Zhang, et al., In-situ measurements of stress evolution in composite sulfur cathodes, Energy Storage Mater 16 (2018) 491–497.
[30] K. Zhao, M. Pharr, J.J. Vlassak, Z. Suo, Fracture of electrodes in lithium-ion batteries caused by fast charging, J. Appl. Phys. 108 (2010) 1–7.
[31] H. Ye, Y.X. Yin, Y.G. Guo, Insight into the loading temperature of sulfur on sulfur/carbon cathode in lithium-sulfur batteries, Electrochim. Acta 185 (2015) 62–68.
[32] M.R. Busche, et al., Systematical electrochemical study on the parasitic shuttle-effect in lithium-sulfur-cells at different temperatures and different rates, J. Power Sources 259 (2014) 289–299.
[33] J.W. Park, et al., Solvent effect of room temperature ionic liquids on electrochemical reactions in lithium-sulfur batteries, J. Phys. Chem. C 117 (2013) 4431–4440.
[34] L. Yuan, X. Qiu, L. Chen, W. Zhu, New insight into the discharge process of sulfur cathode by electrochemical impedance spectroscopy, J. Power Sources 189 (2009) 127–132.
[35] W. Tang, et al., In situ observation and electrochemical study of encapsulated sulfur nanoparticles by MoS2Flakes, J. Am. Chem. Soc. 139 (2017) 10133–10141.
[36] H. Kim, et al., In situ TEM observation of electrochemical lithiation of sulfur confined within inner cylindrical pores of carbon nanotubes, Adv. Energy Mater. 5 (2015) 1–7.
[37] Z. Yuan, et al., Powering lithium-sulfur battery performance by propelling polysulfide redox at sulfiphilic hosts, Nano Lett. 16 (2016) 519–527.
[38] J.Q. Huang, et al., Ionic shield for polysulfides towards highly-stable lithium-sulfur batteries, Energy Environ. Sci. 7 (2014) 347–353.
[39] S. Bai, X. Liu, K. Zhu, S. Wu, H. Zhou, Metal-organic framework-based separator for lithium-sulfur batteries, Nat. Energy 1 (2016).
[40] H. Yao, et al., Improved lithium-sulfur batteries with a conductive coating on the separator to prevent the accumulation of inactive S-related species at the cathode-separator interface, Energy Environ. Sci. 7 (2014) 3381–3390.
[41] M. Pharr, Z. Suo, J.J. Vlassak, Variation of stress with charging rate due to strain-rate sensitivity of silicon electrodes of Li-ion batteries, J. Power Sources 270 (2014) 569–575.
[42] M. Pharr, Z. Suo, J.J. Vlassak, Measurements of the fracture energy of lithiated silicon electrodes of Li-Ion batteries, Nano Lett. 13 (2013) 5570–5577.
[43] M. Pharr, Y.S. Choi, D. Lee, K.H. Oh, J.J. Vlassak, Measurements of stress and fracture in germanium electrodes of lithium-ion batteries during electrochemical lithiation and delithiation, J. Power Sources 304 (2016) 164–169.
[44] G.R. Hardin, Y. Zhang, C.D. Fincher, M. Pharr, Interfacial fracture of nanowire electrodes of lithium-ion batteries, JOM (J. Occup. Med.) 69 (2017) 1519–1523.